Mine Water Environ (2016) 35:18–28
DOI 10.1007/s10230-015-0327-7

TECHNICAL ARTICLE

Removal of Toxic Metal Ions from Sungun Acid Rock Drainage Using Mordenite Zeolite, Graphene Nanosheets, and a Novel Metal–Organic Framework

Esmaeil Rahimi · Neda Mohaghegh

Received: 9 June 2014 / Accepted: 31 January 2015 / Published online: 12 February 2015

Abstract We evaluated the sorptive properties of mordenite zeolite (MOR), a copper terephthalate metal–organic framework (MOF), and graphene oxide (GO) and their potential use in treating acid rock drainage (ARD) containing Fe^{3+}, Cu^{2+}, Mn^{2+}, Zn^{2+}, Pb^{2+}, and Cd^{2+} ions. MOR was prepared via a hydrothermal method, MOF was prepared via a solvothermal method, and few-layered GO nanosheets were synthesized using Hummers' method. The aqueous contaminants were removed by chemico-physical sorption and ion exchange in batch tests. It proved possible to dramatically improve removal efficiency and sorptive capacity by optimizing experimental conditions. Magnetic MOF crystals were more efficient in removing metals than the MOR and GO. Sorption tests using ARD from the Sungun copper mine and a multi-component solution containing cationic metal species revealed that both GO nanosheets and magnetic MOF have great potential for ARD treatment.

Keywords Graphene oxide · Sorption process · Sungun copper mine

Electronic supplementary material The online version of this article (doi:10.1007/s10230-015-0327-7) contains supplementary material, which is available to authorized users.

E. Rahimi (✉)
Department of Mining Engineering,
Islamic Azad University–South Tehran Branch,
1639664981 Tehran, Iran
e-mail: SE_Rahimi@azad.ac.ir

N. Mohaghegh
Department of Chemistry, Sharif University of Technology,
Azadi Ave, Tehran, Iran
e-mail: mohaghegh@ch.sharif.edu

Introduction

The generation of acid rock drainage (ARD) and the release of dissolved metals into the environment are crucial concerns for the mining industry (Motsi et al. 2009). ARD is a prevalent source of environmental pollution and often contains metals such as: Cu^{2+}, Fe^{3+}, Mn^{2+}, Zn^{2+}, Cd^{2+}, and Pb^{2+} (Mayer et al. 2006; Vermaak et al. 2006). Some of these metals can be toxic or carcinogenic and accumulate in living organisms (Matlock et al. 2002; Kalin et al. 2006). Therefore, their removal from waste and tailings effluent could have significant benefits for human health and the environment.

Metal ions can be removed from water using various methods, including solvent extraction, precipitation, vacuum evaporation, membrane filtration, ion exchange, and adsorption (Gupta et al. 2006, 2007a, b, 2009). Method selection is based on the concentration of metal ions in the aqueous solution and the cost of treatment.

Adsorption is simple, economical, and efficient. Sorbents such as clay minerals, zeolite, blast furnace slag, and activated carbon have been studied extensively for ARD treatment (Motsi et al. 2009; Namasivayam and Yamuna 1999; Peric et al. 2004; Ŕıos et al. 2008). However, these sorbents suffer from either low sorption capacities or other inefficiencies. Nanomaterials can resolve some of these problems due to their high surface area, increased active sites, and abundant functional surface groups. Nanomaterials such as carbon nanotubes, zeolite nanocrystals, and graphene nanosheets have high sorptive capacities (Chandra et al. 2010; Long and Yang 2001; Wang et al. 2008; Zhao et al. 2011a) and have been widely used to remove different kinds of organic and inorganic pollutants from large quantities of aqueous solution.

Zeolites (crystalline aluminosilicates) with uniform pore size and extensive surface area have been used in ARD

treatment system design. The use of natural and synthetic zeolites as sorbents has gained interest because zeolites provide a combination of ion exchange and molecular sieve properties that can be easily modified (Shiokawa et al. 1989).

Graphene, a type of atomic-layered graphite, possesses a special two-dimensional structure and excellent mechanical, thermal, and electrical properties. Graphene and its derivatives have high surface areas (a theoretical value of 2,600 m^2/g for exfoliated graphene sheets) and many functional groups on the surface that contribute to metal ion removal.

Metal–organic frameworks (MOFs) are crystalline porous materials consisting of metal ions coordinated by organic ligands to form rigid three-dimensional frameworks. MOFs with unique properties, such as large surface area, low framework density, magnetic properties, and high pore volume, have considerable promise in adsorption processes. To the best of our knowledge, there are no reports on the application of copper terephthalate MOF material as an adsorbent. This novel magnetic MOF can be reasonably easily incorporated into conventional water treatment materials, opening a new option for water purification. The use of synthesized graphene oxide (GO) nanosheets, mordenite zeolite (MOR), and novel MOF crystals is of special interest in both adsorption processes and ARD treatment based on their unique structure, high surface area, biocompatibility, and mesoporous properties. We studied the sorption characteristics and uptake efficiency of Fe^{3+}, Cu^{2+}, Mn^{2+}, Zn^{2+}, Cd^{2+}, and Pb^{2+} ions from aqueous solutions and ARD from the Sungun copper mine using nanocrystalline MOR, copper terephthalate MOF, and GO nanosheets.

Experimental

Materials

Sodium silicate (Na_2SiO_3), aluminium nitrate [$Al(NO_3)_3 \cdot 3H_2O$], and sodium hydroxide (NaOH) were obtained from Merck for MOR synthesis. Terephthalic acid (tpaH), copper nitrate ($Cu(NO_3)_2 \cdot 3H_2O$), and N,N-dimethylformamide (DMF) were purchased from Merck for MOF synthesis. For the GO synthesis, graphite powder was purchased from Fluka and concentrated sulphuric acid (H_2SO_4), potassium persulphate ($K_2S_2O_8$), diphosphorus pentaoxide (P_2O_5), hydrogen peroxide (H_2O_2), and potassium permanganate ($KMnO_4$) were obtained from Merck. Synthetic solutions with metal ions were prepared using their respective metal salts. All metal salts and other chemicals were of the highest purity available and were obtained from Merck. An ARD sample provided by the Sungun copper mine was used to test MOR, MOF, and GO activity.

Instruments

For detecting the mineral phases, the XRD pattern of the prepared MOR and MOF was recorded using a Philips X'pert instrument operating with Cu Kα irradiation ($\lambda = 0.15406$ nm) as the X-ray source. The absorption spectrum of GO was determined by UV–Vis spectrophotometer (GBC Cintra 40). The average particle size and morphology of prepared samples were distinguished by scanning electron microscopy (SEM, XL30 model). FT-IR spectra in the range of 4,000–400 cm^{-1} were reported in the transmission mode on an ABB BOMER MB series spectrophotometer. The specific surface area and pore volume distributions of the prepared samples were calculated from the nitrogen adsorption–desorption isotherms at 77 K using a Belsorp apparatus. Metal ion content was analysed by atomic absorption (AA, Varian SpectrAA 220 spectrometer).

Catalyst Preparation

Synthesis of Copper Terephthalate MOF

Solvothermal synthesis of the Cu (tpa) (dmf) MOF was performed as described by Cantwell et al. (2009). For the MOF crystal synthesis, copper nitrate trihydrate and tpaH were dissolved in DMF with vigorous stirring. The reaction mixture was heated in an oil bath at 140 °C overnight to yield cubic crystals of MOF. It is worth noting that the framework of MOF particles requires tight control of the thermal conditions. After completing the synthesis, the resultant blue product was collected by filtration, washed, and dried.

Synthesis of MOR

Nanocrystalline MOR was prepared by a two-step hydrothermal method (Mohaghegh et al. 2014). First, a gel containing silica and aluminium species was prepared in a 400 mL Borosil beaker by dissolving finely divided silica and aluminium in an alkaline hydroxide solution. To achieve uniform small particles and complete mixing, the gel was magnetically stirred for 2 h. Then, the resulting product was rapidly transferred into a Teflon-lined stainless steel autoclave under autogenous pressure and static conditions. After natural cooling to room temperature, the product was collected using a centrifuge and washed until the pH of the remaining solution was <9. The white powder was collected, dried, and then calcined at 550 °C for 8 h. The synthetic zeolite was denoted as MOR and stored in powder form for further use.

Synthesis of GO

Few-layered GO nanosheets were synthesized by oxidation of natural graphite powder according to a modified Hummers' method. In the first step, 3.00 g of graphite powder was added to a mixture of concentrated H_2SO_4, $K_2S_2O_8$, and P_2O_5. After that, the prepared mixture was heated to 80 °C and allowed to react for 6 h. Then, oxidized graphite was made by diluting the solution with deionized water (DI), filtered using nylon Millipore film, repeatedly washed with DI, and finally dried in air overnight. In the second step, 460 mL of H_2SO_4 was added to the oxidized graphite and stirred. Afterward, 6 g of $KMnO_4$ was added slowly at constant temperature, and then stirred for 2 h at 35 °C. Next, 920 mL of DI was added slowly to the suspension while keeping the temperature below 50 °C. After 2 h, DI and H_2O_2 were added to the mixture, which was centrifuged and washed with HCl solution, followed by 5 mL of DI to eliminate the acid. Lastly, the resulting product was subjected to dialysis for a week to remove acids, and dried under vacuum conditions (Li and Wu 2009). GO nanosheets obtained from the oxidation of graphite powder are readily dispersed in polar solvents such as DI.

Sorption Experiments

Sorption experiments were done in a batch reactor. In this set-up, the reactor was surrounded by a circulating water jacket to maintain a constant 25 °C. Two hundred mL of synthesized solution, including metal ions with the desired concentration and 0.1 g of adsorbents, were fed into the reactor. The suspension was magnetically stirred at 300 rpm for 120 min. 4 mL of solution was withdrawn from the reactor, centrifuged for 10 min at 10,000 rpm, and submitted for AA analysis. By performing a proper material balance, the quantity of ions adsorbed at regular time intervals was determined spectrophotometrically for kinetic analysis.

Results and Discussion

Characterization of Sorption Materials

UV–Vis Spectra of GO

UV–Vis absorption spectrum of GO is represented in supplementary Fig. 1, which accompanies the on-line version of this paper. The absorption peak around 235 nm is assigned to the $\Pi \rightarrow \Pi^*$ transitions of C=C bonds, and a shoulder, at about 290–300 nm, relates to the $n \rightarrow \Pi^*$ transition of the C=O bond (Zhou et al. 2009).

XRD Analysis

The XRD pattern of MOR is depicted in supplementary Fig. 2. The average crystal size for MOR calcined at 550 °C was calculated to be 30 nm from half the width of the diffraction peaks by applying Scherrer's formula (Lipson and Steeple 1970). The zeolitic phases were recognized by comparing the diffraction peaks with data in the ICSD database (Pankaj et al. 2008). The XRD pattern of copper terephthalate MOF (supplementary Fig. 3) show that the MOF crystals were successfully formed, because the diffraction peaks can all be readily indexed to Cu(tpa)(dmf) (Cantwell et al. 2009).

BET Analysis

Table 1 indicates the surface area and total pore volume data for the prepared samples. It has been suggested that GO, MOF, and MOR can be used as adsorbents. High specific surface area is usually required to enhance the adsorption efficiency of metal ions. The GO and novel MOF material have the highest specific surface area, indicating their potential for adsorbing metal ions. However, the surface area is still lower for GO than the theoretical value for completely exfoliated and isolated GO sheets because of incomplete exfoliation and agglomeration of GO sheets after fast heat treatment. This is consistent with the SEM image of the GO sheets being randomly aggregated and crumpled. Agglomeration of GO sheets can arise from fractional coalescing. Agglomeration reduces the specific surface area, but the crumpled structure still leaves a large exposed surface area (Stankovich et al. 2007).

FE-SEM Analysis

FE-SEM was used to investigate the surface morphology of the prepared samples. The SEM images of the prepared GO nanosheets, MOR, and MOF nanocrystals are shown in Figs. 1, 2, and 3, respectively. Two magnifications of the MOR nanoparticles (Fig. 1a, b) below the calcination temperature (550 °C) show that the MOR nanoparticles were approximately 32 nm in size and were homogeneously dispersed.

The synthesized GO sample (Fig. 2) consists of randomly aggregated, thin, crumpled sheets nearly associated

Table 1 Properties of the synthesized sorbents

Adsorbents	S_{BET} (m^2g^{-1})	Total pore volume (cm^3g^{-1})
MOR	322.0	0.214
GO	478.7	1.313
MOF	573.0	0.481

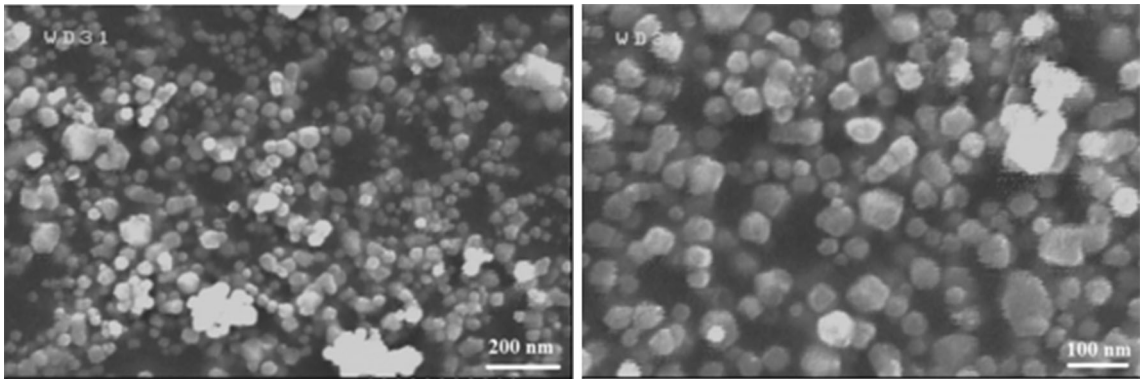

Fig. 1 SEM images of synthesized MOR nanoparticles calcined at 550 °C

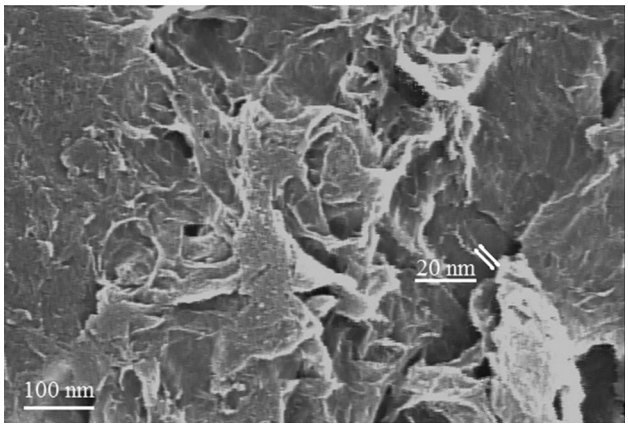

Fig. 2 The SEM image of aggregated GO sheets

with each other and generating a disordered sample. The folded regions of the nanosheets were determined from the SEM image to have average widths of ≈54 nm. At the resolution limit of our instrument, this image also shows that individual sheets exist in the GO sample. This qualitative conclusion was further confirmed by BET analysis. The MOF crystal sample obviously exhibits three dimensional cubic structures, with a relatively smooth surface, showing that the preparation conditions were suitable for synthesizing MOF crystals (Fig. 3).

FT-IR Spectroscopy

Supplementary Fig. 4 represents the FT-IR spectrum of MOR nanocrystals calcined at 550 °C. The bands in the regions of 400–520 cm^{-1}, 7,100–830 cm^{-1}, and 1,000–1,050 cm^{-1} belong to the asymmetric and symmetric stretching mode of the T–O–T bond and stretching mode of the T–O bond in SiO_4 and AlO_4 structures, respectively (T = Si, Al). The band around 3,400 cm^{-1} corresponds to O–H stretching, meaning that MOR nanocrystals physically adsorb water from the air (Pankaj et al. 2008).

Supplementary Fig. 5 displays the FT-IR spectrum of the GO nanosheets. The main oxygen-containing groups on the GO surface expected to form strong surface complexes with metal ions were characterized; the specific peaks indicate that large numbers of oxygen-containing functional groups exist on these surfaces (Zhao et al. 2011b). Similarly, supplementary Fig. 6 shows the FT-IR spectrum

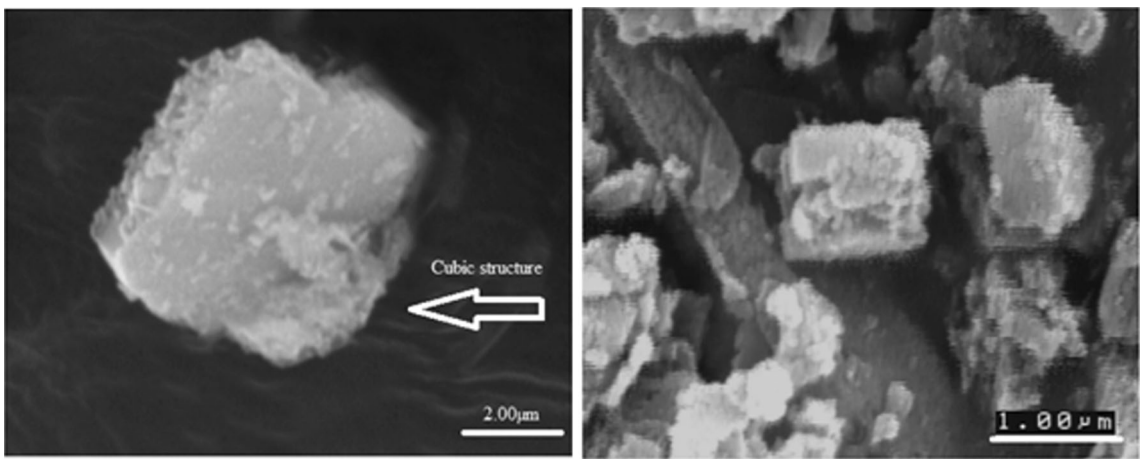

Fig. 3 The SEM image of MOF crystal

of the MOF crystals. The bands in the regions of 1,640 cm^{-1}, 2,940 cm^{-1}, and 1,430–1,550 cm^{-1} belong to the C=O, C–H groups, and –O–C–O–, respectively (Cantwell et al. 2009); the peaks indicate that large numbers of functional groups exist on the MOF crystal surfaces.

Sorption of Metal Ions Over Synthesised MOR, MOF, and GO

Figure 4 shows the sorption curves of Fe^{3+}, Cu^{2+}, Mn^{2+}, Zn^{2+}, Cd^{2+}, and Pb^{2+}. It can be seen that the removal efficiency for total ions by MOF crystals and GO nanosheets was higher than for the MOR sorbent. This is thought to be due to the higher specific surface area of the synthetic MOF and GO. In addition, when MOF was used as a sorbent, the metal ions appeared to be chemically sorbed by functional groups in the MOF. As a result, MOF crystals with many functional groups, such as –O–C–O–, carboxylate ligands, and C=O, can complex with the metal ions. Generally, the highly porous framework of MOF crystals enables guest molecules such as metal ions to diffuse into the MOF structure; the shape and size of the pores leads to selectivity over the guests that may be adsorbed. These features make MOF an ideal sorbent for removal of metal ions from aqueous solution. Finally, MOF with magnetic properties can be separated by an external magnetic field and repeatedly reused in metal ion removal (Cantwell et al. 2009).

The lower specific surface area of MOR compared to MOF and GO was approximately compensated for by MOR's unique structure. MOR has additional transporting channels that provide a desirable pathway for ion exchange. The metal ions in the MOR transport channels were exchanged with the metal ions in the solution. With regard to GO, the high sorption activity of GO nanosheets is attributed to the interconnected pore structure being conducive to ion diffusion. When GO was used as a sorbent, in addition to the high specific surface area, metal ions were chemically sorbed by surrounding the metal ions with epoxides, hydroxides, carboxylic groups, and carboxylate on the surface of the GO sheets. As a result, GO with many functional groups, such as –O–, –OH, and –COOH, can complex with the metal ions (Zhao et al. 2011a). Moreover, the metal ions accumulate along the wrinkles and edges on the GO surface (Zhang et al. 2010). Therefore, GO, with more oxygen-containing groups and higher specific surface area, had a higher adsorptive capacity than MOR.

In all of the prepared samples, it was observed that the removal efficiency for Cu^{2+} was higher than for other ions. The radius of Cu^{2+} is less than Zn^{2+}, Cd^{2+}, and Pb^{2+}, making it more suitable for effective ion exchange in both

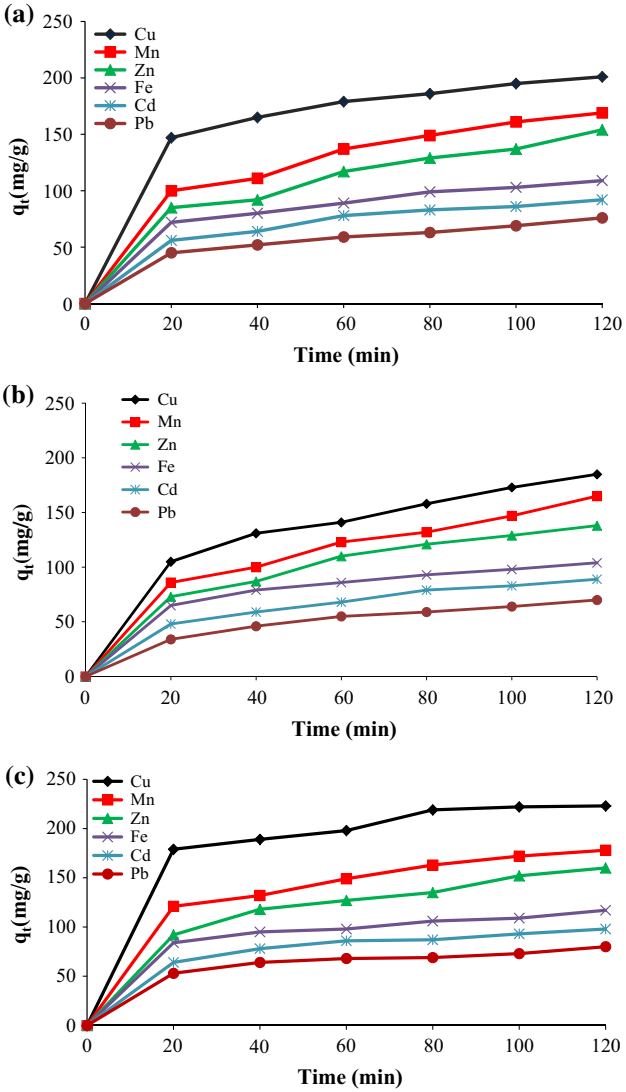

Fig. 4 Removal efficiency of metal ions from synthetic solution with **a** GO nanosheets, **b** MOR nanocrystals, and **c** MOF crystals (pH = 7, contact time = 120 min, T = 25 °C)

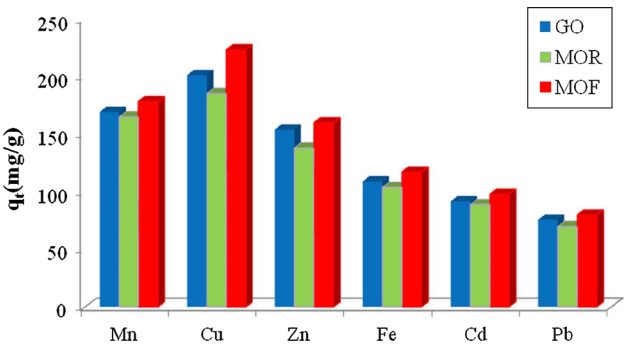

Fig. 5 The adsorption activity of prepared MOR, MOF, and GO (pH = 7, contact time = 120 min, T = 25 °C)

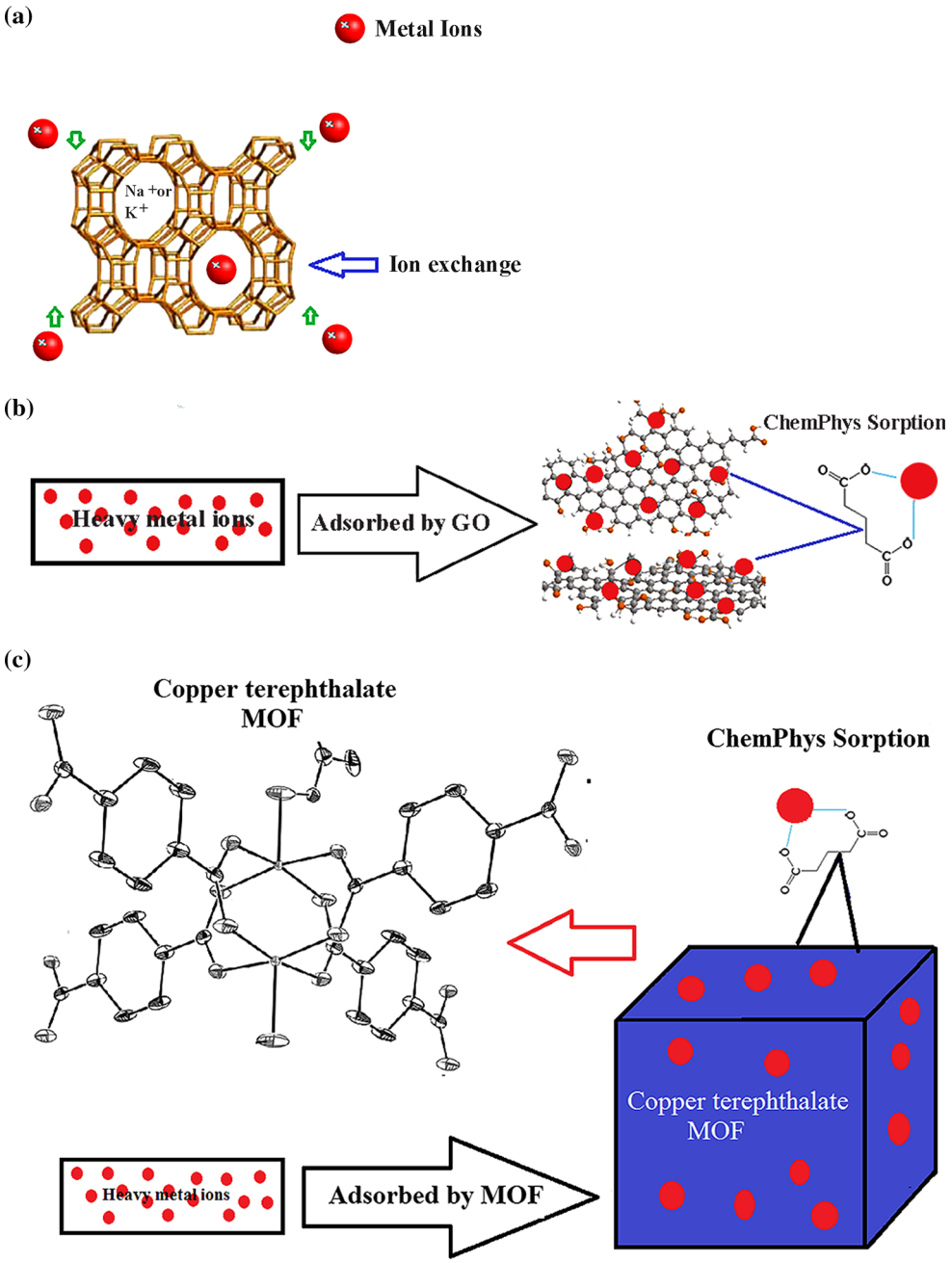

Fig. 6 Total removal process of metal ions with prepared **a** MOR nanocrystals, **b** GO nanosheets, and **c** MOF crystals

the MOR and MOF structures and promoting more effective bonding with functional groups on both GO and MOF surfaces (Motsi et al. 2009).

The adsorption activity of the MOR, MOF, and GO sorbents is represented in Fig. 5. MOF crystals and GO nanosheets show higher adsorption capacity due to having more functional groups on the surface, high surface area, and a unique framework.

For all of the prepared samples, adsorption is a heterogeneous process with an initially fast adsorption phase, when more active sites are available for the ions to interact with; ion exchange in the pores of sorbent grains and adsorption on the sorbent's surface also occurs during this stage. Adsorption is also faster at first since the driving force for adsorption, which is the concentration difference between the bulk solution and the solid–liquid interface, is initially very high (Inglezakis et al. 2002). However, after this initial period, adsorption slows, possibly due to diffusion of metal ions into the interior channels of both MOR and MOF and into available pores on the GO surface and MOF crystals. In this later stage, ions occupy exchangeable positions within the crystal structure of MOR and MOF. Figure 6 illustrates the total metal removal process with MOR, MOF nanocrystals, and GO nanosheets.

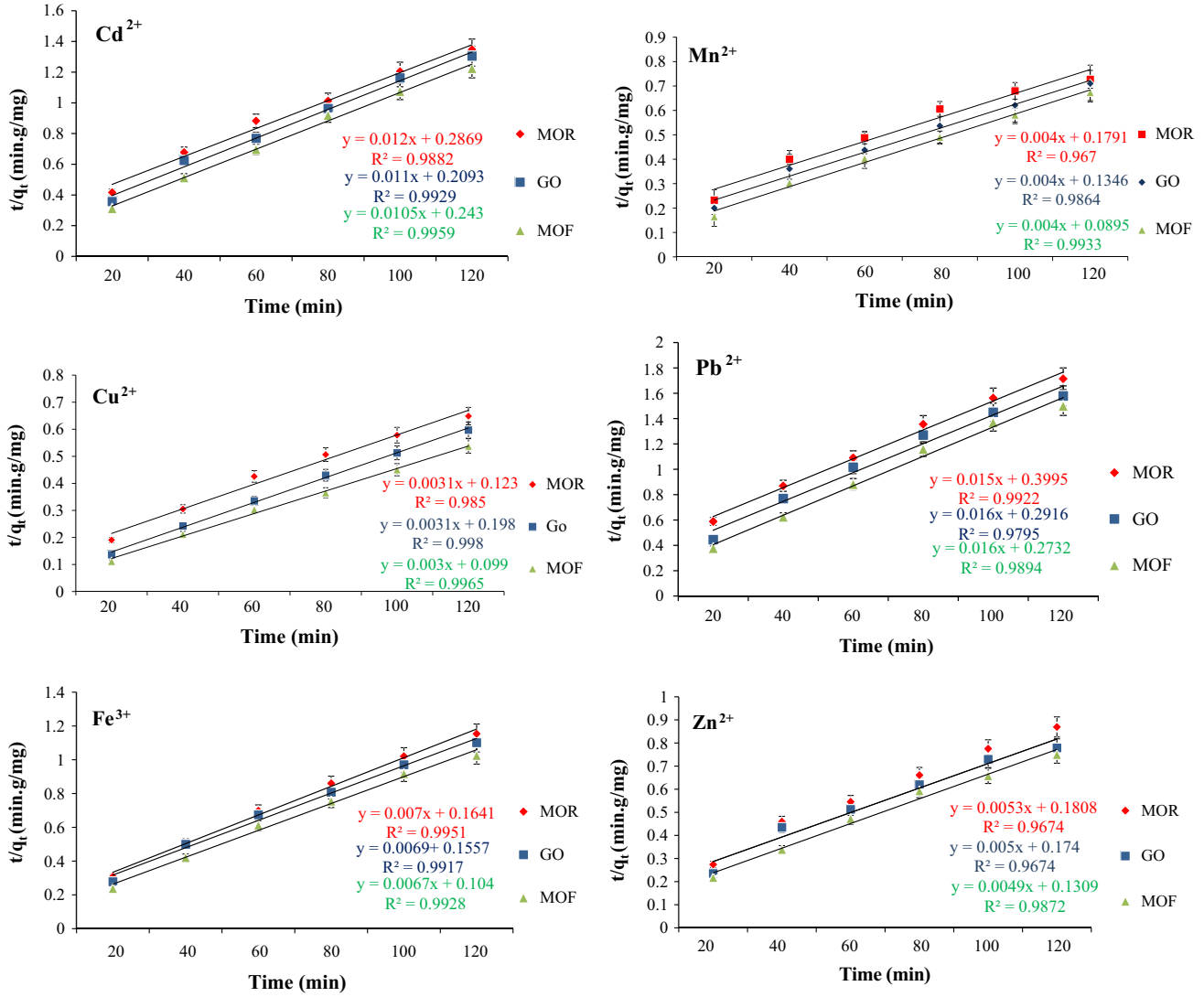

Fig. 7 Pseudo-second-order kinetic plots for ion sorption onto MOR, MOF, and GO samples

Kinetic Analysis

Kinetic sorption plots of metal ions on the prepared MOR, MOF, and GO sorbents are represented in Fig. 7. A pseudo-second order rate expression was the best fit for the total metal ions, which is consistent with the assumption that the determining rate step may be chemical sorption consisting of valence forces created by sharing or electronic interaction between the adsorbent and adsorbate (Motsi et al. 2009; Ŕıos et al. 2008; Taty-Costodes et al. 2003). The pseudo-second-order chemisorption kinetics law for the reaction is expressed as:

$$\frac{dq_t}{dt} = k(q_e - q_t)^2 \tag{1}$$

Separating the variables in Eq. 1 gives

$$\frac{dq_t}{(q_e - q_t)^2} = kdt \tag{2}$$

where q_e is that amount of solute adsorbed per unit mass at equilibrium, q_t is the amount of metal ions adsorbed at time t (mg g^{-1} adsorbent) and k is the second order rate constant (g $mg^{-1}min^{-1}$). A linear form of the typical second-order rate equation is summarized as Eq. 3:

$$\frac{t}{q_t} = \frac{1}{h} + \frac{1}{q_e}t \tag{3}$$

and h is calculated from Eq. 4.

$$h = kq_e^2 \tag{4}$$

The pseudo-second-order model constants can be calculated experimentally by plotting $\frac{t}{q_t}$ versus time (t).

Sorption Isotherms

The above equations very precisely describe the wide range of results presented in this paper and it is believed that they can be widely applied to analyse the isotherm data. Langmuir and Freundlich isotherm models are both used in analysis of adsorption. The Freundlich isotherm model is an empirical model that can be used for non-ideal sorption that contains heterogeneous systems, but the Langmuir isotherm model is considered by the authors to be the best available for describing sorption and has been successfully applied to many sorption processes (Motsi et al. 2009; Ŕıos et al. 2008). In this research, the sorption data for Cu^{2+} ion with the MOF crystal adsorbent were fitted into the linearized Langmuir equation (Eq. 5); the results can be seen in Table 2 and Fig. 8.

$$\frac{C_e}{q_e} = \frac{1}{q_m} C_e + \frac{1}{bq_m} \quad (5)$$

where C_e is the metal ion concentration (mg L^{-1}) at equilibrium, q_e is the amount of metal ions adsorbed per gram of adsorbent at equilibrium (mg g^{-1} adsorbent), b and q_m are the Langmuir constants assigned to the energy of adsorption and the maximum adsorption capacity, respectively. The coefficients q_m (mg g^{-1} adsorbent) and b (mg^{-1}) can be estimated from a plot of C_e/q_e versus C_e.

Table 2 Langmuir constants at three different temperatures for Cu^{2+} ion onto the *MOF* crystals

Temperature/°C	R^2	Eqs.	Q_m	B
25	0.971	Y = 0.0139X + 0.24	71.94	0.058
30	0.960	Y = 0.0117X + 0.22	85.47	0.053
35	0.981	Y = 0.0109X + 0.24	91.74	0.045

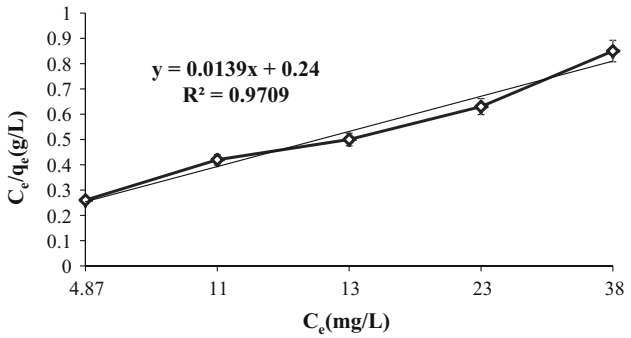

Fig. 8 Linearized Langmuir isotherm (Eq. 5) for Cu^{2+} sorption in the presence of MOF crystals (contact time = 120 min, T = 25 °C)

Effect of pH

The pH affects the adsorption of metal ions by GO, MOR, and MOF sorbents by affecting the solubility of the metal ions, ion concentration in the functional groups of adsorbents, and ionization degree of the adsorbate in the sorption process. The removal efficiency of metal ions for prepared adsorbents was increased by initially increasing solution pH (Fig. 10). Active sites on MOR nanocrystals can be preferentially protonated or deprotonated depending on the pH. Holistically, more H^+ ions are adsorbed from solution in more acidic conditions. For example, Zn exists as Zn^{2+}, $ZnOH_2^+$, and $Zn(OH)_4^{2-}$, depending on pH. MOR is generally weakly acidic and sodium form exchangers are highly selective for H^+ ions, as summarized in Eq. 6 (Erdem et al. 2004; Inglezakis et al. 2003; Sprynskyy et al. 2006):

$$R - Na + H_2O \rightarrow RH + Na^+ + OH^- \quad (6)$$

This reaction takes place at high pH. At an acidic pH, H^+ ions compete with metal ions for exchange sites in MOR

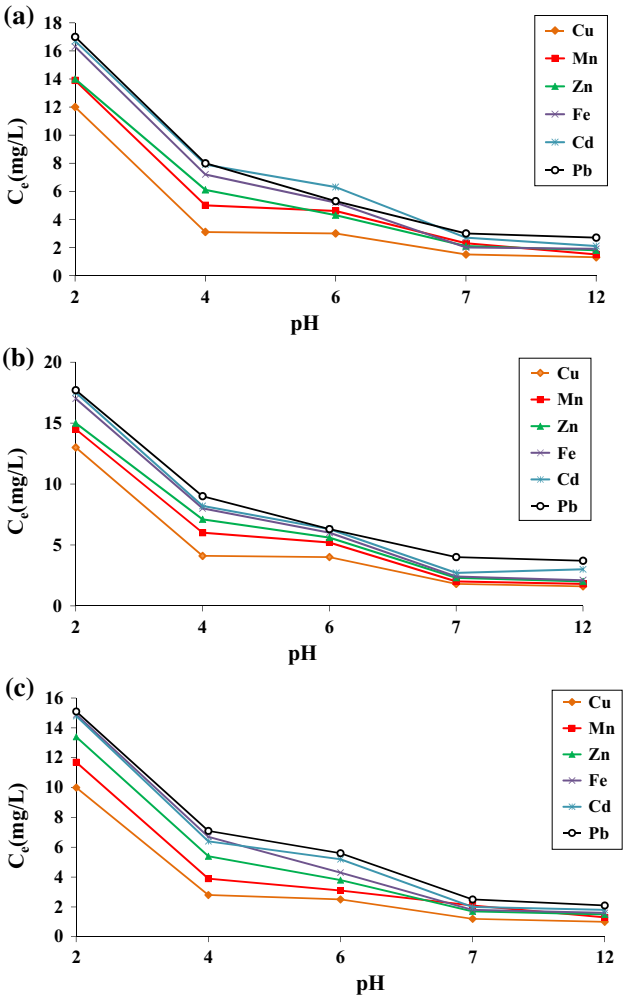

Fig. 9 Effect of pH on the ion sorption in the presence of **a** GO, **b** MOR, and **c** MOF (contact time = 120 min, T = 25 °C)

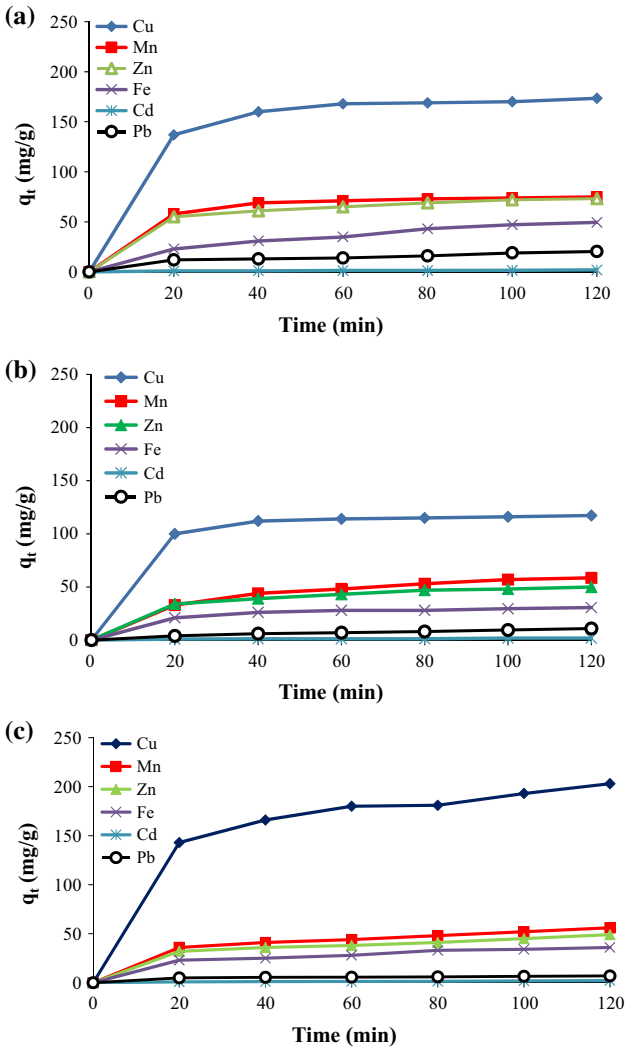

Fig. 10 Removal efficiency of metal ions from Sungun Copper Mine wastewater with: **a** GO nanosheets, **b** MOR nanocrystals, and **c** MOF crystals

pores and channels. In contrast, the MOR surface is positively charged at low pH. At higher pH, the H^+ concentration is less, allowing more metal ions to be adsorbed, as shown by decreasing C_e in Fig. 9b.

For both GO nanosheets and MOF crystals, the functional groups on the adsorbent surface are expected to remain more anionic at higher pH; this can significantly contribute to metal ion removal via chemsorption. At $pH < pH_{pzc}$ (pH of point of zero charge), the surface charge of both MOF and GO is positive due to protonation (Eq. 7). Positive metal ions fail to adsorb on the positively charged surface of both MOF and GO nanoadsorbents because of electrostatic repulsion. At $pH > pH_{pzc}$, the surface charge of both MOF and GO is negative due to the deprotonation (Eq. 8).

$$\_SOH + H^+ \rightarrow \_SOH_2^+ \quad (7)$$

$$\_SOH \rightarrow \_SO^- + H^+ \quad (8)$$

where _S shows the nanosorbent surface and _OH shows the oxygen-containing functional groups (Zhao et al. 2011a). The reaction for hydroxide formation of metal ions (M^{2+}) is summarized in Eq. 9.

$$M^{2+} \leftrightarrow M(OH)^+ \leftrightarrow M(OH)_2^0 \leftrightarrow_- M(OH)^- \quad (9)$$

Metal ions can also combine with deprotonated surface sites, allowing sorption on nanosorbents (Eq. 10).

$$2\_SO^-_{(s)} + M^{2+}_{(eq)} \rightarrow \left[(\_SO^-)_2 M^{2+}\right]_{(s)} \quad (10)$$

The pH influences speciation of the surface functional groups as well as the degree of deprotonation and protonation. At an enhanced pH, the adsorbent surface becomes more negative and electrostatic interactions between the metal ions and nanoadsorbents become stronger, increasing metal ion removal (Zhao et al. 2011c).

Removal of Metal Ions from Natural ARD

Tests were conducted using pH 3.7 ARD wastewater collected from a low grade sulphide deposit in the Sungun copper mine to evaluate the sorptive activity of prepared samples (Figs. 10, 11). One thousand mL of ARD and 0.1 g of adsorbents were fed into the reactor. The Cu^{+2}, Mn^{+2}, Cd^{+2}, Zn^{+2}, Fe^{+3}, and Pb^{+2}

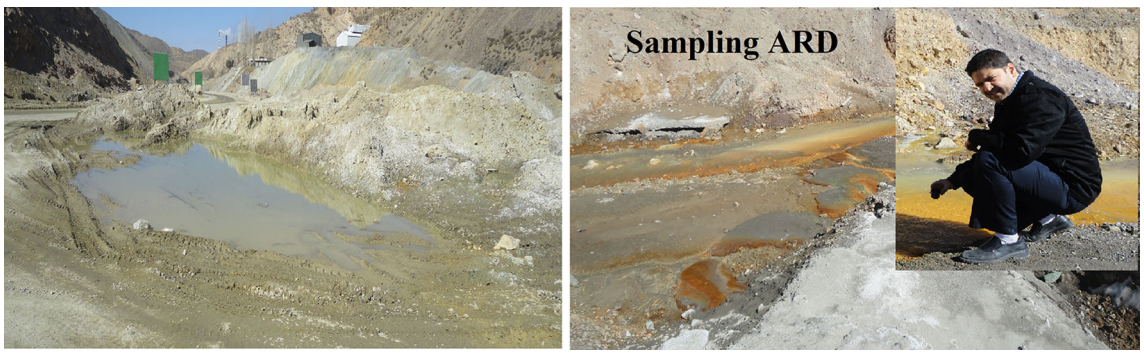

Fig. 11 ARD sampling from the Sungun Copper Mine

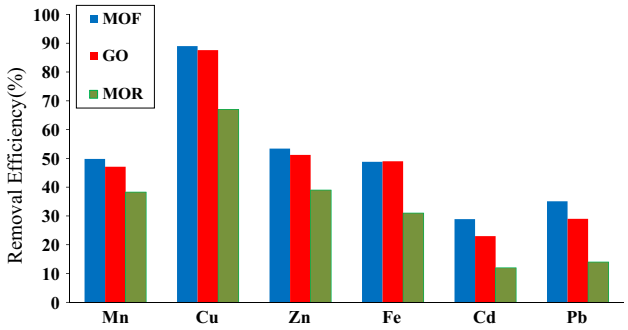

Fig. 12 Comparison of ARD removal efficiency among nanosorbents

concentrations in the Sungun ARD sample were 228.1, 112.4, 35.9, 91.7, 73.7, and 35.1 mg/L, respectively. Finally, the removal efficiency of the MOF, GO, and MOR nanosorbents for treating Sungun ARD wastewater was compared (Fig. 12). The MOF crystals and GO nanosheets showed high total metal removal efficiency.

Conclusions

Nanocrystalline MOR, MOF, and few-layered GO nanosheets were prepared and characterized using various techniques. The adsorbents were used to remove metal ions from a prepared aqueous solution and from ARD from the Sungun copper mine. The results revealed that sorbent properties, such as high surface area, recoverability, unique structures, and specific functional groups, strongly influenced removal efficiency. Analysis of sorption kinetics and isotherms showed that ion removal obeyed pseudo-second-order kinetics and Langmuir models, respectively. Increasing the initial pH of the solution increased removal efficiency; this is believed to be due to ion exchange capacity, speciation of the surface functional groups, and degree of deprotonation. Consequently, the highest sorption activity was observed for both MOF nanocrystals and GO nanosheets due to their high surface area, unique framework, and various functional groups distributed on the surfaces of the nanosorbents. Copper terephthalate MOF is a novel sorbent that shows impressive removal of metal ions from aqueous solution. In addition, MOF has magnetic properties and can be separated from solution by an external magnetic field and repeatedly reused. The sorptive activity of both Cu(tpa) (dmf) MOF crystals and GO was clearly superior to the MOR sorbent for ion removal from aqueous solution and natural ARD.

Acknowledgments The authors are grateful to Mr. Rezai from the Sungun Copper Mine for providing an ARD wastewater sample.

References

Chandra V, Park J, Chun Y, Lee JW, Hwang IC, Kim KS (2010) Water-dispersible magnetite-reduced graphene oxide composites for arsenic removal. ACS Nano 4:3979–3986

Erdem E, Karapinar N, Donat R (2004) The removal of heavy metal cations by natural zeolite. J Colloid Interface Sci 280:309–314

Gupta VK, Mittal A, Krishnan L, Mittal J (2006) Adsorption treatment and recovery of the hazardous dye, brilliant blue FCF, over bottom ash and de-oiled soya. J Colloid Interface Sci 293:16–26

Gupta VK, Ali I, Saini VK (2007a) Defluoridation of wastewaters using waste carbon slurry. Water Res 41:3307–3316

Gupta VK, Singh AK, Gupta B (2007b) Schiff bases as cadmium (II) selective ionophores in polymeric membrane electrodes. Anal Chem Acta 583:340–348

Gupta VK, Goyal RN, Sharma RA (2009) Novel PVC membrane based alizarin sensor and its application; determination of vanadium, zirconium and molybdenum. Int J Electrochem Sci 4:156–172

Inglezakis VJ, Loizidou MD, Grigoropoulou HP (2002) Equilibrium and kinetic ion exchange studies of Pb^{2+}, Cr^{3+}, Fe^{3+} and Cu^{2+} on natural clinoptilolite. Water Res 36:2784–2792

Inglezakis VJ, Loizidou MD, Grigoropoulou HP (2003) Ion exchange of Pb^{2+}, Cu^{2+}, Fe^{3+} and Cr^{3+} on natural clinoptilolite: selectivity determination and influence of acidity on metal uptake. J Colloid Interface Sci 261:49–54

Kalin M, Fyson A, Wheeler WN (2006) The chemistry of conventional and alternative treatment systems for the neutralization of acid mine drainage. Sci Total Environ 366:395–408

Li Y, Wu Y (2009) Coassembly of graphene oxide and nanowires for large-area nanowire alignment. J Am Chem Soc 131:5851–5857

Lipson H, Steeple H (1970) Interpretation of X-ray Powder Diffraction Patterns. Macmillan, London

Long RQ, Yang RT (2001) Carbon nanotubes as superior sorbent for dioxin removal. J Am Chem Soc 123:2058–2059

Matlock MM, Howerton BS, Atwood DA (2002) Chemical precipitation of heavy metals from acid mine drainage. Water Res 36:4757–4764

Mayer KU, Benner SG, Blowes DW (2006) Process-based reactive transport modeling of a permeable reactive barrier for the treatment of mine drainage. J Contam Hydrol 85:195–211

Mohaghegh N, Tasviri M, Rahimi E, Gholami MR (2014) Nano sized ZnO composites: preparation, characterization and application as photocatalysts for degradation of AB92 azo dye. Mater Sci Semicond Process 21:167–179

Motsi T, Rowson NA, Simmons MJH (2009) Adsorption of heavy metals from acid mine drainage by natural zeolite. Int J Miner Process 92:42–48

Namasivayam C, Yamuna RT (1999) Studies on chromium (III) removal from aqueous solution by adsorption onto biogas residual slurry and its application to tannery wastewater treatment. Water Air Soil Pollut 113:371–384

Pankaj S, Rajaram P, Tomar R (2008) Synthesis and morphological studies of nanocrystalline MOR type zeolite material. J Colloid Interface Sci 325:547–557

Peric J, Trgo M, Vukojevic-Medvidovic N (2004) Removal of zinc, copper and lead by natural zeolite—a comparison of adsorption isotherms. Water Res 38:1893–1899

Ŕıos CA, Williams CD, Roberts CL (2008) Removal of heavy metals from acid mine drainage (AMD) using coal fly ash, natural clinker and synthetic zeolites. J Hazard Mater 156:23–35

Shiokawa K, Ito M, Itabashi K (1989) Crystal structure of synthetic mordenite zeolites. Zeolites 9:170–176

Sprynskyy M, Buszewski B, Terzyk AP, Namiesnik J (2006) Study of the selection mechanism of heavy metal (Pb^{2+}, Cu^{2+}, Ni^{2+} and Cd^{2+}) adsorption on clinoptilolite. J Colloid Interface Sci 304:21–28

Stankovich S, Dikin DA, Piner RD, Kohlhaas KA, Kleinhammes A, Jia Y, Wu Y, Nguyen ST, Ruoff RS (2007) Synthesis of graphene-based nanosheets via chemical reduction of exfoliated graphite oxide. Carbon 45:1558–1565

Taty-Costodes VC, Fauduet H, Porte C, Delacroix A (2003) Removal of Cd(II) and Pb(II) ions, from aqueous solutions, by adsorption onto sawdust of Pinus sylvestris. J Hazard Mater 105:121–142

Vermaak SSP, Potgieter JH, Monama P, Grieken RV (2006) Comparison of limestone, dolomite and fly ash as pre-treatment agents for acid mine drainage. Miner Eng 19:454–462

Wang XL, Lu JL, Xing BS (2008) Sorption of organic contaminants by carbon nanotubes: influence of adsorbed organic matter. Environ Sci Technol 42:3207–3212

Zhang H, Lv X, Li Y, Wang Y, Li J (2010) P25-graphene composite as a high performance photocatalyst. ACS Nano 4:380–386

Zhao GX, Jiang L, He Y, Li JX, Dong HL, Wang XK, Hu WP (2011a) Sulfonated graphene for persistent aromatic pollutant management. Adv Mater 23:3959–3963

Zhao GX, Li J, Ren X, Chen Ch, Wang X (2011b) Few-layered graphene oxide nanosheets as superior sorbents for heavy metal ion pollution management. Environ Sci Technol 45:10454–10462

Zhao GX, Ren XM, Gao X, Tan XL, Li JX, Chen CL, Huang YY, Wang XK (2011c) Removal of Pb(II) ions from aqueous solutions on few-layered graphene oxide nanosheets. Dalton Trans 40:10945–40952

Zhou Y, Bao Q, Tang LAL, Zhong Y, Loh KP (2009) Hydrothermal dehydration for the "Green" reduction of exfoliated graphene oxide to graphene and demonstration of tunable optical limiting properties. Chem Mater 21:2950–2956